Am J Physiol Heart Circ Physiol 294: H1417–H1425, 2008.
First published January 25, 2008; doi:10.1152/ajpheart.01233.2007.

Spatially discordant alternans in cardiomyocyte monolayers

Carlos de Diego, Rakesh K. Pai, Amish S. Dave, Adam Lynch, Mya Thu, Fuhua Chen, Lai-Hua Xie, James N. Weiss, and Miguel Valderrábano

Cardiovascular Research Laboratory, Departments of Medicine (Cardiology), Pediatrics (Cardiology), and Physiology, David Geffen School of Medicine at University of California Los Angeles, Los Angeles, California

Submitted 23 October 2007; accepted in final form 21 January 2008

de Diego C, Pai RK, Dave AS, Lynch A, Thu M, Chen F, Xie L-H, Weiss JN, Valderrábano M. Spatially discordant alternans in cardiomyocyte monolayers. *Am J Physiol Heart Circ Physiol* 294: H1417–H1425, 2008. First published January 25, 2008; doi:10.1152/ajpheart.01233.2007.—Repolarization alternans is a harbinger of sudden cardiac death, particularly when it becomes spatially discordant. Alternans, a beat-to-beat alternation in the action potential duration (APD) and intracellular Ca (Ca_i), can arise from either tissue heterogeneities or dynamic factors. Distinguishing between these mechanisms in normal cardiac tissue is difficult because of inherent complex three-dimensional tissue heterogeneities. To evaluate repolarization alternans in a simpler two-dimensional cardiac substrate, we optically recorded voltage and/or Ca_i in monolayers of cultured neonatal rat ventricular myocytes during rapid pacing, before and after exposure to BAY K 8644 to enhance dynamic factors promoting alternans. Under control conditions ($n = 37$), rapid pacing caused detectable APD alternans in 81% of monolayers, and Ca_i transient alternans in all monolayers, becoming spatially discordant in 62%. After BAY K 8644 ($n = 28$), conduction velocity restitution became more prominent, and APD and Ca_i alternans developed and became spatially discordant in all monolayers, with an increased number of nodal lines separating out-of-phase alternating regions. Nodal lines moved closer to the pacing site with faster pacing rates and changed orientation when the pacing site was moved, as predicted for the dynamically generated, but not heterogeneity-based, alternans. Spatial APD gradients during spatially discordant alternans were sufficiently steep to induce conduction block and reentry. These findings indicate that spatially discordant alternans severe enough to initiate reentry can be readily induced by pacing in two-dimensional cardiac tissue and behaves according to predictions for a predominantly dynamically generated mechanism.

calcium cycling; arrhythmias

T-WAVE ALTERNANS, AN IMPORTANT marker of arrhythmia risk (25), arises from beat-to-beat alternation in the electromechanical response at the cellular level (18). Alternans can be spatially concordant, when the entire tissue alternates in phase, or spatially discordant, when adjacent regions alternate out of phase, separated by a nodal line at which no alternation occurs. Spatially discordant alternans amplifies dispersion of repolarization and can precede conduction block and reentry in whole heart mapping studies (12, 13, 18). Two mechanisms have been proposed to explain how alternans becomes spatially discordant in cardiac tissue: *1*) inherent heterogeneous tissue properties, including structural (19), electrophysiological (14, 18), and/or intracellular calcium (Ca_i) cycling (20) heterogeneities; and *2*) dynamic factors, such as steep action potential (AP) duration (APD) restitution slope or a Ca_i cycling instability, in combination with conduction velocity (CV) restitution (9, 23, 26–28, 31). Since both factors are naturally present in real cardiac tissue, it has been difficult to evaluate their relative importance in producing alternans. Recent modeling studies, however, have suggested criteria by which the behavior of nodal lines in response to pacing interventions can be used to distinguish between these mechanisms (9, 31). These criteria, applied to intact rabbit ventricles (9), supported a key role of dynamic factors in the genesis of spatially discordant alternans. However, in three-dimensional (3D) studies in which only the surface can be mapped, it cannot be excluded that unmapped subsurface events may influence the properties of spatially discordant alternans.

Neonatal rat ventricular myocyte monolayers provide a simple two-dimensional (2D) tissue model to explore the relevance of dynamic factors to spatially discordant alternans. Here we used optical mapping of membrane voltage and Ca_i in monolayers to determine whether spatially discordant alternans could be induced, and, if so, whether its behavior supported a role of dynamic factors. In addition to control conditions, we studied the effects of the L-type Ca current agonist BAY K 8644, which enhances dynamic factors by steepening APD restitution slope and promoting Ca_i cycling instability by loading the sarcoplasmic reticulum (SR) with high levels of Ca. Our findings provide strong additional experimental support for the role of dynamic factors in the generation of spatially discordant alternans and directly demonstrate that spatially discordant alternans can lead to conduction block and initiation of reentry in a preparation without any unmapped subsurface tissue.

METHODS

Monolayer Preparation

Neonatal rat ventricular myocytes from 2- to 3-day-old Sprague-Dawley rats were obtained by standard methods (24), plated on 22 × 22-mm plastic coverslips (10^6 myocytes per coverslip), and cultured for 6–7 days. Monolayers with insufficient cellular confluence, as assessed by phase-contrast microscopy, or uneven propagation patterns during pacing at 2 Hz were excluded from analysis. Monolayers were studied under two different conditions: control ($n = 37$) and during exposure to BAY K 8644 (racemic, 0.1 μM, Sigma, $n = 28$). The use and care of the animals in these experiments were approved by the Chancellor's Animal Research Committee at the University of California Los Angeles.

Stimulation Protocol

Unipolar point stimuli were delivered at the edge of the coverslip using a Grass stimulator triggered by computer-controlled pacing sequences. Specimens were paced at 2 Hz. Then a rapid pacing

Address for reprint requests and other correspondence: J. N. Weiss, Division of Cardiology, 3645 MRL Bldg., David Geffen School of Medicine at UCLA, Los Angeles, CA 90095 (e-mail: jweiss@mednet.ucla.edu).

The costs of publication of this article were defrayed in part by the payment of page charges. The article must therefore be hereby marked "*advertisement*" in accordance with 18 U.S.C. Section 1734 solely to indicate this fact.

protocol was performed, initially at 340-ms cycle length, decremented by 20 ms every eight beats until reaching 140-ms cycle length.

Optical Mapping System

Monolayers were stained by immersion into oxygenated Tyrode's solution (in mM, 136 NaCl, 5.4 KCl, 1.8 $CaCl_2$, 0.33 NaH_2PO_4, 1 $MgCl_2$, 10 HEPES, and 10 glucose, pH 7.3) at 37°C, containing the fluorescent voltage dye RH-237 (5 μM for 5 min) and/or the Ca dye rhod 2-AM or rhod-FF (5 μM for 40 min) plus 0.016% (wt/wt) pluronic (Molecular Probes, Eugene, OR), and then placed in a perfusion bath. Experiments were conducted at 37°C. Fluorescence was excited by two light sources (each with 4 light-emitting diodes; Luxeon, Ontario, Canada) filtered at 540 ± 20 nm. The emitted fluorescence was separated using a dichroic mirror (at 630 nm), directed to two separate cameras with their corresponding emission filters (715 nm for RH-237 and 585 nm for rhod 2/rhod-FF).

Charge-coupled device camera recordings. We used electron-multiplying, back-illuminated, cooled charge-coupled device (CCD) cameras (Photometrics Cascade 128+), with 128 × 128 spatial resolution at 0.6- to 5-ms per frame. Signals were digitized with 16 bits of precision. Single-dye staining with rhod 2-AM (n = 22) or RH-237 (n = 19) confirmed the absence of cross talk between voltage and Ca signals, and simultaneous voltage and Ca mapping were performed in 15 specimens.

Photodiode array. In nine additional experiments, voltage (RH-237 staining) was also recorded optically using a photodiode array (PDA) (WuTech), consisting of 464 hexagonally arranged sites with 720-μm spacing.

Data Analysis

Raw data were processed with custom-written software. When the goal was to optimize spatial resolution (at the expense of temporal resolution), CCD recordings were subjected to *1*) spatial filter (2 × 2 binning); *2*) 5-point median temporal filter; *3*) polynomial curve fitting to eliminate baseline drift caused by photobleaching; and *4*) range normalization. After processing, this yielded a final spatial resolution of 64 × 64 (340 × 340 μm/pixel) and a temporal resolution of 15–25 ms (3–5 ms per frame × 5). When the goal was to optimize temporal resolution (at the expense of spatial resolution), CCD recordings were subjected to spatial filter (4 × 4 binning), and the other same algorithms were applied. This yielded a postprocessing spatial resolution of 32 × 32 (680 × 680 μm/pixel) and a final temporal resolution of 3 ms (0.6 ms per frame × 5). As an alternative method to enhance temporal resolution, we also used PDA recordings in place of CCD recordings in some experiments, with no spatial or temporal filtering applied to the PDA traces.

APD was measured at 80% repolarization (APD_{80}) using custom-written software to detect the time to repolarize to 80% from the peak amplitude of the AP back to the take-off point of the same AP. This may have modestly underestimated the amplitude of APD alternans when the take-off point was also alternating, but did not affect the detection of the onset or offset of APD alternans. We chose APD_{80} rather than APD at 90% repolarization (APD_{90}) to minimize measurement ambiguity when full repolarization was not achieved at rapid pacing rates. Diastolic interval (DI) was measured from 80% repolarization of the previous AP to the next AP upstroke. Ca_i transient amplitude was measured as the absolute increase in fluorescence (minimum to peak in arbitrary units). APD and Ca_i alternans were considered to be present when APD_{80} and Ca_i transient amplitude alternated by >10 ms and >10%, respectively, on a beat-to-beat basis, and persisted until the end of the pacing protocol. Difference maps between APD_{80} and Ca_i transient amplitude on successive beats were generated and shaded red if the differences were positive, and green if negative. Thus, during spatially discordant alternans, red and green regions alternated, separated by a nonalternating nodal line (white). CV was estimated using voltage signal with custom-written software, which detected the activation time of each pixel and measured the difference in activation time between two points separated by a known distance located orthogonally to propagation direction. To avoid artifacts from direct activation of myocytes near the pacing site (virtual electrode), CV was calculated from the average difference in activation time between a site 5 mm from the pacing site and three equidistant sites as remote as possible from the pacing site. APD_{80} and CV restitution curves were generated by plotting APD_{80} or CV vs. DI and fitting to a single exponential. APD restitution slopes were calculated by differentiating the exponential fits using Origin (Microcal) software. Maximum APD restitution slope was obtained by calculating the value of this slope at the shortest DI that elicited an AP. The conduction block at the nodal line was defined as block within 1 mm of the nodal line.

Statistics

Data are shown as means ± SD. Statistical tests included χ^2 test and Student's T-test. P values <0.05 were considered significant.

RESULTS

Electrophysiological Properties Before and After BAY K 8644

We examined 37 monolayers under control conditions, with optical mapping of Ca_i alone (n = 10), voltage alone (n = 16), or both simultaneously (n = 11). A bright-field image of a representative confluent monolayer meeting our inclusion criteria is shown in Fig. 1*A*. Figure 1*B* shows representative optical traces of membrane voltage [voltage fluorescence (F_V)] and Ca_i [Ca_i fluorescence (F_{Ca})]. APD averaged 126 ± 12 ms, and Ca_i transient duration (full width at half-maximal amplitude) averaged 174 ± 14 ms. In all monolayers meeting our

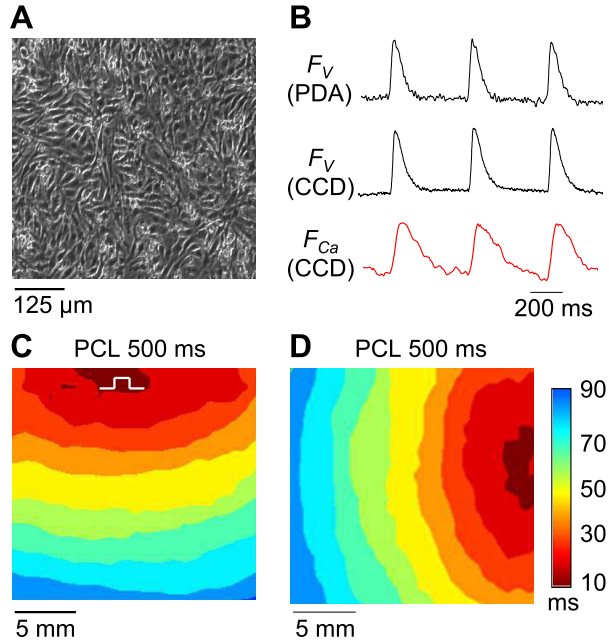

Fig. 1. Cardiomyocyte monolayers. *A*: phase-contrast microphotograph of a typical cardiomyocyte monolayer meeting the inclusion criteria of homogeneous confluence. *B*: representative optical voltage [voltage fluorescence (F_V)] traces [photodiode array (PDA) or charge-coupled device (CCD) camera as labeled, using RH-237] and intracellular Ca (Ca_i) [Ca_i fluorescence (F_{Ca})] trace (CCD camera, using rhod 2-AM) from representative sites in a monolayer. *C* and *D*: isochronal maps obtained from the voltage data show uniform propagation during pacing at 500-ms pacing cycle length (PCL) from orthogonal pacing sites at the *top* (*C*) or *right* (*D*) side of the same monolayer.

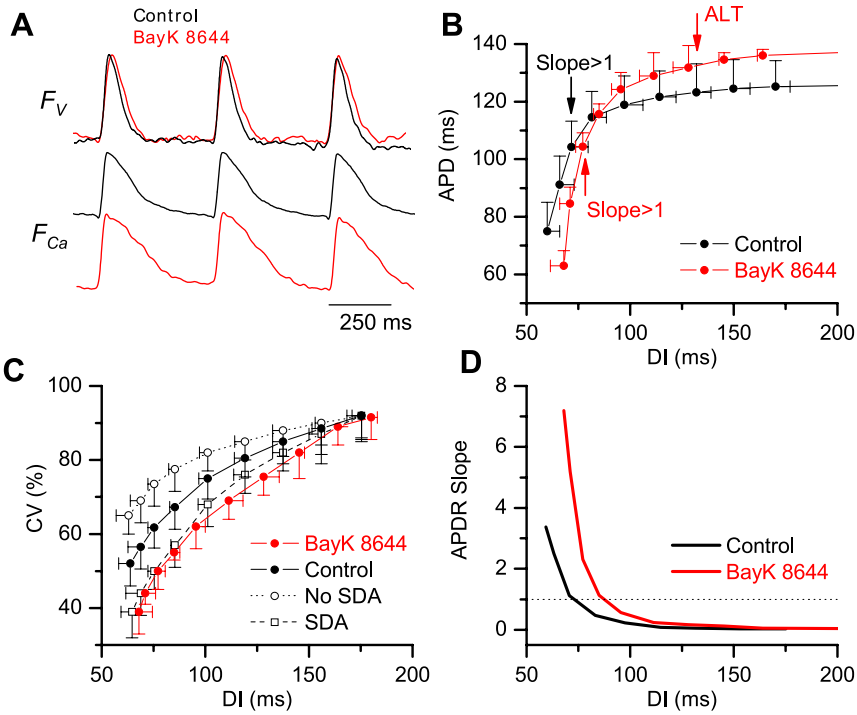

Fig. 2. Action potential duration (APD) and conduction velocity (CV) restitution curves before and after BAY K 8644. *A*: optical F_V and F_{Ca} traces before (black) and after (red) BAY K 8644. APD at 80% repolarization (APD_{80}) and Ca_i transient amplitude increased after BAY K 8644. (Changes in diastolic F_{Ca} after BAY K 8644 could not be measured accurately due to photobleaching.) *B*: dynamic APD restitution (APDR) curve [APD vs. diastolic interval (DI)] before (black) and after (red) BAY K 8644. The onset of APD alternans after BAY K 8644 is indicated by the red arrow (ALT). The DI at which APDR slope exceeds 1 (Slope $>$ 1) before (black arrow) and after (red arrow) BAY K 8644 is also shown. Note that the APDR slope was $<$ 1 at the onset of APD alternans. *C*: CV restitution before (solid black line and symbols) and after (solid red line and symbols) BAY K 8644. Also shown are the CV restitution curves in monolayers that did (dashed line and open squares) or did not (dotted line and open circles) develop spatially discordant alternans (SDA) before BAY K 8644. All monolayers developed SDA after BAY K 8644. For all cases, CV is shown as a percentage of its value at 500-ms PCL. *D*: slope of APDR vs. DI calculated from monoexponential fits, before (black) and after (red) BAY K 8644. Dotted line indicates slope = 1.

inclusion criteria, propagation was uniform without conduction block when paced at 2 Hz from either of two orthogonally positioned sites (Fig. 1, *C* and *D*). CV averaged 0.24 ± 0.1 m/s in both orthogonal directions.

Figure 2, *A* and *B*, shows the effects of BAY K 8644 on APD_{80} and Ca_i transient amplitude and duration. During pacing at 2 Hz, BAY K 8644 increased APD_{80} by 11% from 126 ± 12 to 141 ± 19 ms ($P < 0.05$). The net amplitude of the Ca_i transient fluorescence signal increased by 14 ± 8% ($P < 0.05$), which is likely to be an underestimate of the change in absolute Ca concentration during the Ca_i transient due to the nonlinearity of the dye. The Ca_i transient duration increased by 32% from 178 ± 24 to 235 ± 52 ms ($P <$ 0.05). After BAY K 8644, CV during pacing at 2 Hz was similar to control (0.21 ± 0.03 vs. 0.24 ± 0.04 m/s, P = not significant). Figure 2*B* compares APD restitution curves before and after BAY K 8644. Maximum APD restitution slope averaged 3.0 ± 0.9 under control conditions and 7.2 ± 1 after BAY K 8644 (Fig. 2*B*). The range of DIs over which APD restitution slope was $>$ 1 was 73–59 ms (corresponding to pacing cycle lengths ≤ 180 ms) in control conditions, and 85–68 ms (corresponding to pacing cycle lengths ≤ 200 ms) after BAY K 8644 (Fig. 2*D*). Figure 2*C* shows that significant CV restitution was present (solid black line), and CV was further reduced by BAY K 8644 at short DIs (red line).

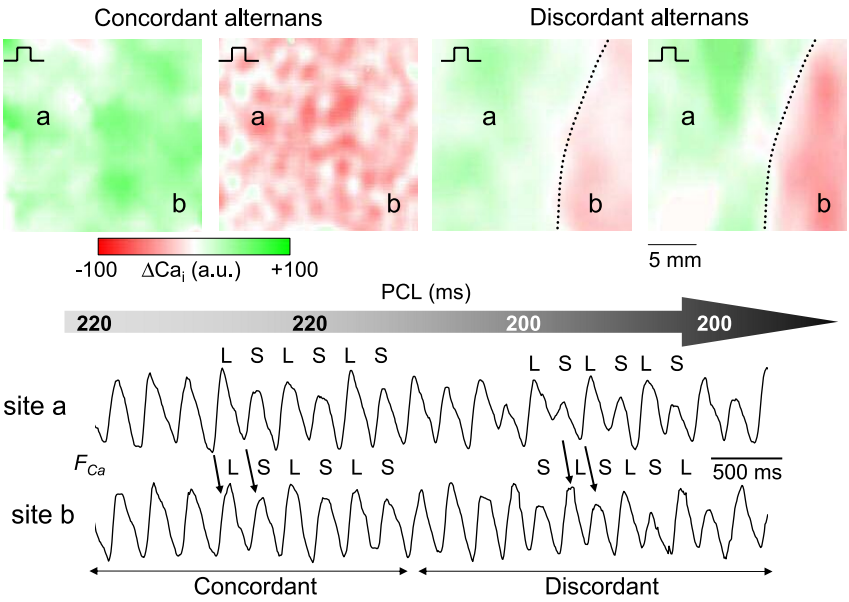

Fig. 3. Spatially concordant and discordant Ca_i transient alternans during rapid pacing. *Top*: spatial patterns of Ca_i transient alternans over the surface of a monolayer for two successive beats during pacing at 220 ms (two *left* panels) and 200 ms (two *right* panels). Red and green indicate positive and negative beat-to-beat changes in Ca_i transient amplitude, respectively. At 220-ms PCL, alternans is spatially concordant (i.e., alternans map shows all green on the first beat, and all red on the next beat). As PCL was shortened to 200 ms, alternans became spatially discordant. Two areas (green and red) alternated out of phase, separated by a white nodal line (NL; dotted line). F_{Ca} traces recorded at *sites a* and *b* in the monolayer (see *top*) show spatially concordant alternans at 220 ms, transitioning to SDA at 200 ms. Large (L) and small (S) Ca_i transients are labeled. Δ, Change; a.u., Arbitrary units.

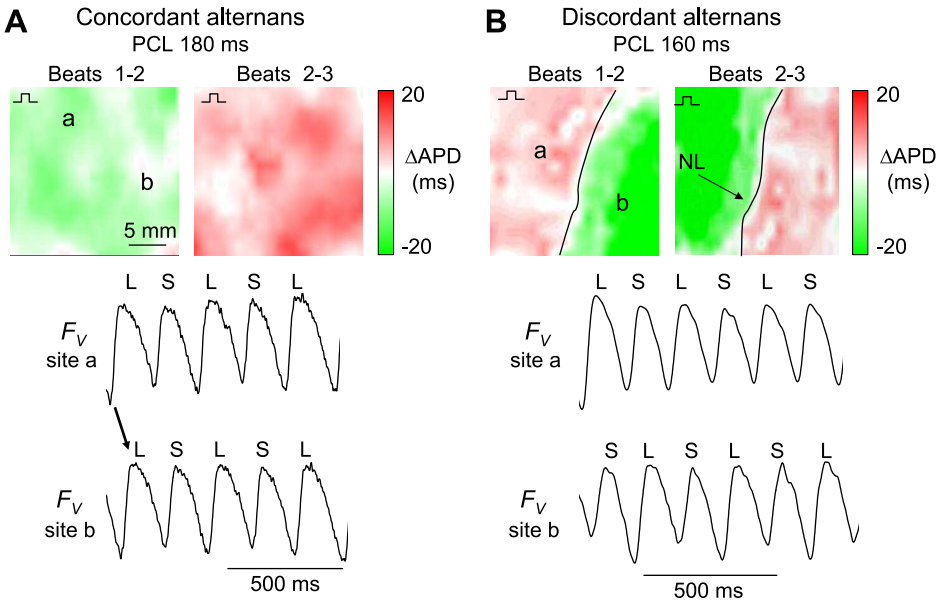

Fig. 4. Spatially concordant and discordant APD alternans during rapid pacing. *A*: spatially concordant APD alternans. APD difference maps between consecutive beats show that the entire tissue alternated in phase at 180-ms PCL. Tracings show optical F_V recordings at *sites a* and *b*, with L and S labels indicating long and short APD, respectively. *B*: spatially discordant APD alternans. APD difference maps between consecutive beats demonstrate two regions alternating out of phase, separated by a NL (black line) oriented perpendicular to propagation direction. Tracings show optical recordings at *sites a* and *b*.

Thus, by increasing the L-type Ca current, BAY K 8644 increased APD and steepened APD restitution slope, increased Ca_i transient amplitude and duration, and caused CV to slow to a greater extent at short DIs. All of these effects are predicted to promote dynamically induced spatially discordant APD and Ca_i alternans (23, 31).

Pacing-induced Ca_i Transient and APD Alternans Under Control Conditions

Spatially concordant and discordant alternans. Monolayers could be paced to a cycle length of 156 ± 14 ms before 1:1 capture was lost. Spatially concordant Ca_i transient alternans was induced in all monolayers, at an average pacing cycle length of 225 ± 16 ms, and became spatially discordant in 13 of 21 specimens (62%) at an average pacing cycle length of 213 ± 16 ms. CV restitution was more prominent in monolayers that transitioned to spatial discordant alternans (Fig. 2*C*, open squares) than in those that did not (open circles). Figure 3 shows an example of the Ca_i transient progressing from spatially concordant to discordant alternans. Since Fast et al. (6, 7) reported that the high-Ca affinity of rhod 2-AM can lead to spuriously prolonged Ca_i transients, we also stained three monolayers with rhod-FF-AM (lower Ca affinity) in place of rhod 2-AM. The incidence or onset of Ca alternans did not differ significantly (data not shown).

Under control conditions, we were limited in our ability to detect APD alternans using the standard high-spatial resolution CCD configuration because of the postprocessing temporal resolution of only 15–25 ms per frame. However, when we sacrificed spatial resolution (see METHODS) to improve the postprocessing temporal resolutions to 3 ms (CCD camera) or 0.6 ms (PDA system), APD alternans was detected in 13 of 16 monolayers (81%). The maximum APD alternans magnitude averaged 18 ± 5 ms and progressed from spatially concordant

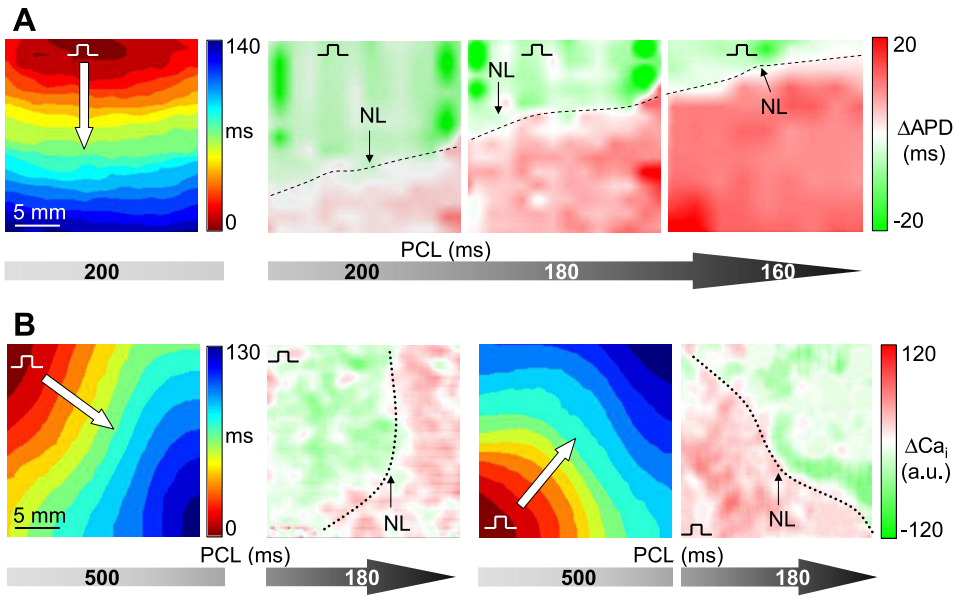

Fig. 5. Effects of PCL and site on NL behavior during spatially discordant APD alternans. *A*: PCL effect on NL position. *Left* panel shows the isochronal activation map during pacing at 200-ms cycle length (note slow CV relative to Fig. 1*B*). *Right* panels show APD difference maps between successive beats at PCLs of 200, 180, and 160 ms. The NL (dashed line) moved progressively closer to the pacing site as the PCL decreased. *B*: pacing site dependence of NL position. *First* and *third* panels show ischronal activation maps when the monolayer was paced at 500-ms cycle length from either the *top left* corner (*first* panel) or *bottom right* corner (*third* panel). *Second* and *fourth* panels show Ca_i transient amplitude difference maps between successive beats during SDA at a PCL of 180 ms for the two different pacing sites. Note that the NL (dashed line) reoriented its position to remain roughly circumferential with respect to the pacing site.

to spatially discordant APD alternans in 8 of 13 monolayers (61%). Figure 4 shows examples.

Nodal line behavior. Theoretical studies (9, 31) predict that during spatially discordant alternans, nodal lines generated dynamically by CV restitution should move closer to the pacing site at faster pacing rates and change their orientation to remain perpendicular to the pacing site when the pacing site is altered, unlike nodal lines due to tissue heterogeneity. We found that APD and Ca_i nodal lines exhibited both of these features. Figure 5*A* shows an example of an APD nodal line moving closer to the pacing site as the pacing cycle length was shortened. Figure 5*B* shows an example of a Ca_i transient nodal line reorienting when the pacing site was moved from the top left to bottom left corner of the monolayer. These findings indicate that nodal lines formed during spatially discordant alternans arise predominantly from a dynamic mechanism, rather than tissue heterogeneity (9).

Effects of BAY K 8644 on APD and Ca_i Transient Alternans

Spatially concordant and discordant alternans. We examined 28 monolayers after exposure to BAY K 8644, mapping either Ca alone ($n = 12$), voltage alone ($n = 12$), or both simultaneously ($n = 4$). After BAY K 8644, 1:1 conduction failed at a longer pacing cycle length of 176 ± 22 ms, compared with 156 ± 14 ms before BAY K 8644 ($P < 0.05$). Spartially concordant Ca_i transient and APD alternans were induced in all (16 of 16) monolayers after BAY K 8644, with the onset at an average pacing cycle of 270 ± 16 ms, compared with 225 ± 6 ms in control conditions ($P < 0.05$). BAY K 8644 also increased the incidence of spatially discordant Ca_i transient and APD alternans from 62 to 100% ($P < 0.01$), which occurred at an average pacing cycle length of 244 ± 16 ms, compared with 213 ± 16 ms before BAY K 8644 ($P < 0.05$). The maximum amplitude of APD alternans was significantly greater (35 ± 6 vs. 18 ± 5 ms in control, $P < 0.05$), as was the maximum amplitude of Ca_i transient alternans (53 ± 14 vs. 35 ± 18% in control, $P < 0.05$).

Nodal line behavior after BAY K 8644. Pacing rate and site had similar effects on nodal line position and orientation after BAY K 8644 (not shown) as under control conditions. BAY K 8644 significantly increased the maximum number of nodal lines. Figure 6 shows an example of multiple APD nodal lines after BAY K 8644. The average number of Ca_i nodal lines increased from 2.1 ± 0.7 to 3.5 ± 0.3 ($P < 0.01$; Fig. 6*C*).), and the average number of APD nodal lines from 2.1 ± 0.4 to 3.1 ± 0.5 ($P < 0.01$; Fig. 6*C*). Thus BAY K 8644 significantly shortened the length scale over which nodal lines formed during spatially discordant Ca_i transient and APD alternans.

Spatially Discordant Alternans, Conduction Block, and Reentry

We next investigated whether spatially discordant alternans could create steep enough APD gradients to cause conduction block and initiation of reentry. Under control conditions, as pacing rate increased, 1:1 conduction with normal propagation was followed by 1:1 conduction with lines of block, and finally 2:1 conduction block, in 11 of 37 specimens (29%). Spatially discordant APD or Ca_i transient alternans preceded the development of lines of conduction block in 81% (9 of 11 specimens), and the site of block occurred near the nodal line in 63% of the cases (7 of 11 specimens). Localized conduction block resulted in initiation of reentry in 6 of 37 specimens (16%).

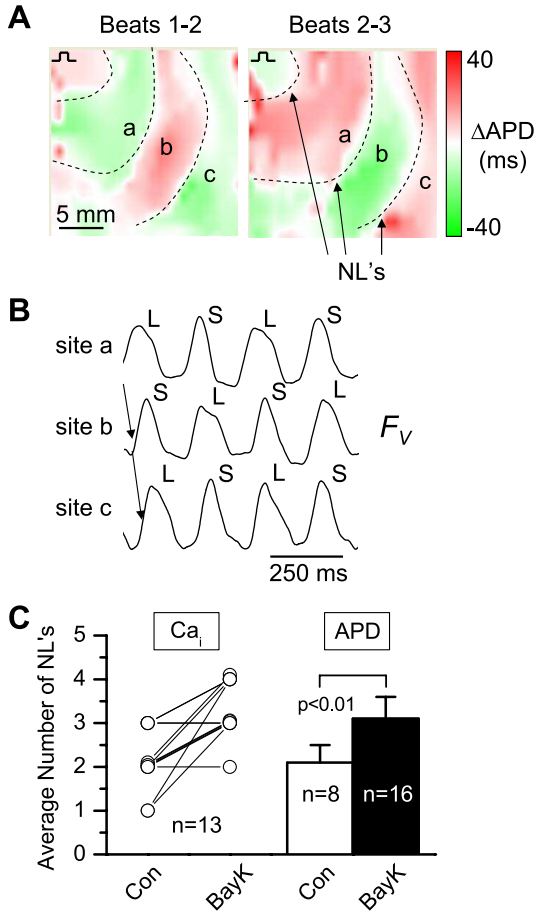

Fig. 6. Effects of BAY K 8644 on NLs. After BAY K 8644, the maximum number of NLs during spatially discordant APD and Ca_i transient alternans increased significantly. *A*: an example from a monolayer during pacing at 200-ms cycle length after BAY K 8644. APD difference maps between two successive pairs of beats (1–2 and 2–3) show three NLs separating 4 regions alternating out of phase. *B*: F_V traces at *sites a*, *b*, and *c* are shown. Bumps in the traces are artifacts, but the alternation between L and S APD is clearly visible. *C*: *left* side compares the number *n* of Ca_i NLs before and after BAY K 8644 in 13 individual preparations. *Right* side shows the average number of APD NLs under control (Con) conditions and after BAY K 8644 obtained from different preparations.

BAY K 8644 increased the incidence of conduction block during rapid pacing to 79% (22 of 28, $P < 0.01$), and lines of block were preceded by spatially discordant alternans in all cases. BAY K 8644 also increased the incidence of reentry during rapid pacing from 16 to 57% (16 of 28 specimens, $P < 0.05$).

The mechanism of conduction block during spatially discordant alternans is illustrated in Fig. 7. After BAY K 8644 exposure, two regions (*sites a* and *b*) alternated out of phase in both Ca_i and APD, separated by a nodal line. Note that the red and green regions of the change (Δ) in Ca_i and ΔAPD maps (Fig. 7*A*) match each other, indicating that larger Ca_i transients are associated with long APD and vice versa. This positive coupling relationship between Ca_i transient amplitude and APD was observed in all monolayers in which voltage and Ca_i were simultaneously recorded, both in control and after BAY

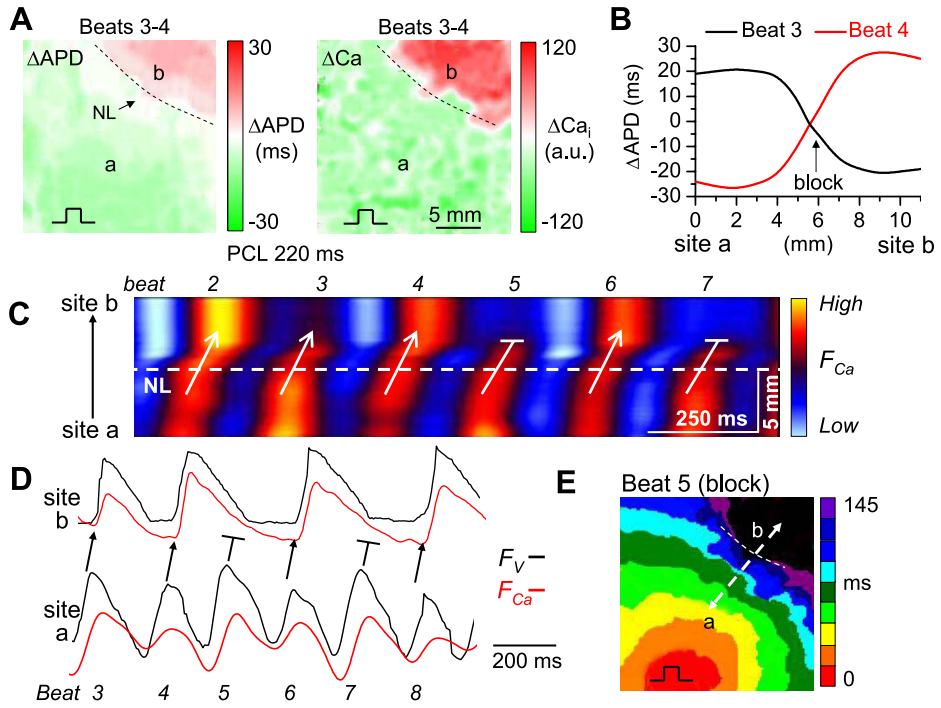

Fig. 7. Conduction block during SDA after BAY K 8644. *A*: simultaneous APD (*left*) and Ca_i transient (*right*) alternans amplitude difference maps for *beats 3–4* during pacing at 220 ms, demonstrating SDA with one NL (dashed line). Note that the red and green regions in the ΔAPD and ΔCa_i maps are matched, indicating that the larger Ca_i transients are associated with longer APD, and vice versa (i.e., positive Ca_i-APD coupling). *B*: the APD gradient along the line between *sites a* and *b* from panel *A* for *beats 3* (black) and *4* (red). The APD gradient was steepest near the NL, reaching 6 ms/mm. *C*: a space-time plot of F_{Ca} for *beats 2–7*. F_{Ca} along the line between *sites a* and *b* is shown on the vertical axis (with red-yellow indicating highest Ca), and time is shown on the horizontal axis. During *beats 2–4*, spatially discordant Ca_i alternans is present, as seen on *beat 3* by the red-yellow F_{Ca}, indicating high Ca amplitude near *site a*, and blue-red F_{Ca} indicating lower Ca amplitude near *site b*, which then reverses on *beat 4*. The NL is indicated by the dashed white line. During *beat 4*, the Ca_i transient is small (corresponding to short APD) near *site a* and large (corresponding to long APD) at *site b*. When the *beat 5* propagates from *site a* toward *b*, in the direction of the increasing Ca_i transient and APD gradient during *beat 4*, conduction block occurs near the NL (dashed white line). *D*: simultaneous optical F_V and F_{Ca} traces at *sites a* and *b* for *beats 3–8*, showing conduction block 2:1 from *beat 5* onwards. Note again the positive coupling relationship between Ca_i transient amplitude and APD. *E*: isochrone activation map illustrating the crowding of isochrone lines before block near *site b* in the *top right* corner.

K 8644. Figure 7*B* shows that, for *beat 3* (black line), APD become shorter as the paced impulse propagated from *site a* with long APD to *site b* with short APD. For *beat 4* (red line), the APD gradient was reversed. As *beat 5* propagated from *site a* to *site b*, the gradient in refractoriness left over from *beat 4* was too steep for successful propagation, causing a line of conduction block to develop close to the nodal line. The graph of APD along the line *ab* in Fig. 7*B* shows that block occurred where the spatial gradient in APD was steepest, reaching 6 ms/mm. Thus *1*) spatially discordant alternans can promote a large enough APD gradient over a 22-mm span in monolayers to induce conduction block (18); *2*) the nodal line marks the location of steepest spatial APD gradient; *3*) conduction block occurs at the nodal line when the new impulse propagates from short-to-long APD direction of the prior beat, which corresponds to the short-to-long Ca_i transient direction (i.e., positive voltage-Ca_i coupling) (29); and *4*) Ca_i transient alternans maps correlate highly with APD alternans maps in their ability to predict the site of nodal lines and conduction block.

Figure 8 illustrates the initiation of reentry in a monolayer exposed to BAY K 8644, using Ca mapping alone. Propagation was initially uniform (Fig. 8*A*). As pacing cycle length decreased to 220 ms, spatially discordant alternans appeared, with three discordantly alternating regions separated by two nodal lines, NL1 and NL2 (Fig. 8*B*). For *beat 5*, unidirectional conduction block occurred immediately past NL1 as the impulse propagated from *site a* toward *site b*, in the small-to-large Ca_i transient direction (corresponding to short-to-long APD direction for positive voltage-Ca^{2+} coupling), as shown in the spatiotemporal plot in Fig. 8*C*. Figure 8*D* shows the isochrome map for *beat 5*, illustrating that conduction block was localized to the central region of the monolayer, allowing propagation around the edges to reenter the region of block from the opposite direction, initiating reentry.

DISCUSSION

Spatially Discordant Alternans in Cardiac Monolayers

The novel findings of this study are that spatially discordant APD and Ca_i alternans *1*) can be induced by rapid pacing in a relatively isotropic 2D cardiac tissue in which the entire surface can be optically mapped, so as to exclude unmapped subsurface electrical activity from influencing the outcome, and can create sufficient repolarization gradients to cause conduction block and reentry; *2*) share features with intact 3D ventricular muscle, indicating that it originates primarily from dynamic factors such as CV restitution (23, 31) rather than tissue heterogeneity; and *3*) are exacerbated by the Ca channel agonist BAY K 8644, as predicted theoretically for an agent

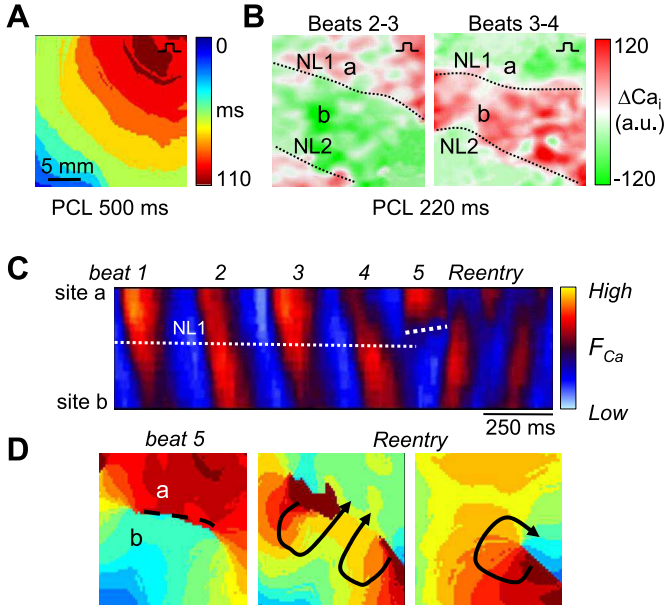

Fig. 8. Conduction block initiating reentry during SDA. *A*: isochrone activation map at a 500-ms PCL, showing uniform propagation after BAY K 8644. F_{Ca} only was recorded in this monolayer. *B*: at 220-ms PCL, Ca_i transient amplitude difference maps between *beats 2–3* (*second* panel) and *beats 3–4* (*third* panel) showed spatially discordant Ca_i alternans, with 2 NLs (NL1 and NL2) separating 3 out-of-phase regions. *C*: space-time plot along the line between *sites a* and *b* shows that conduction block occurred at *beat 5* near NL1 (dashed white line), as the impulse propagated into the region with the larger Ca_i transient on *beat 4* (corresponding to longer APD). The next activation occurs from the opposite direction. *D*: isochrone activation maps for *beats 5*, *6*, and *7* show that conduction block during *beat 5* was localized to the center of the monolayer, allowing *beat 5* to propagate around the edges and reenter the area of conduction block from the other direction, initiating reentry (*beats 6* and *7*).

that steepens APD restitution, promotes Ca_i overload, and increases CV restitution.

The following observations strongly support a dynamic, rather than tissue heterogeneity-based, mechanism in this preparation. *1*) Under control conditions, CV restitution was more prominent in the 62% of monolayers that transitioned from spatially concordant to spatially discordant alternans, compared with the 38% of monolayers that did not (Fig. 2*D*). By increasing CV restitution, BAY K 8644 increased the incidence of spatially discordant alternans to 100%. *2*) BAY K 8644 also increased the number of nodal lines (i.e., decreased the spacing between nodal lines), consistent with theoretical predictions that the length scale of nodal line spacing is decreased by increasing CV restitution and the amplitude of APD alternans (5, 22). *3*) Computer simulations (9, 31) predict that nodal lines generated dynamically by CV restitution should move toward the pacing site as pacing cycle length decreases and should reorient to remain circumferential with respect to the pacing site when the pacing site is changed. In contrast, nodal lines formed as a result of tissue heterogeneity do not share these features (9). In our preparation, we found that nodal lines behaved according to the predictions for the dynamic CV restitution mechanism (Fig. 5), consistent with recent observations on nodal line behavior in intact 3D rabbit ventricular tissue (9). In the case of intact heart tissue, significant macroscopic tissue heterogeneities are unavoidably present. Monolayers, when carefully prepared to be fully confluent, lack gross macroscopic tissue heterogeneity. However, microscopic heterogeneities still exist and may exert important effects. This is evident from our finding that spatially discordant alternans was able to induce localized conduction block (Fig. 8), as required for reentry initiation (rather than circumferential conduction block along the whole wavefront, which cannot induce reentry). The magnitude of the heterogeneity required for this symmetry-breaking effect is unclear. Possibly, it could be very minor at normal heart rates, but amplified by dynamic factors at rapid pacing rates (22), which remains an interesting area to explore in future studies.

Cellular Mechanisms of Repolarization Alternans

Although APD alternans is always dually influenced by both APD restitution steepness (11, 17) and Ca_i cycling dynamics (2, 3), the onset of APD alternans is driven by whichever factor becomes unstable first (29). In neonatal rat ventricular myocyte monolayers, the following observations favor the Ca_i-driven instability as responsible for the onset of alternans. First, the onset of alternans occurred at a pacing cycle length at which APD restitution slope was considerably < 1 (Fig. 2), although short-term memory effects (30) or transient alternans (see below) might conceivably account for this. Second, under control conditions, the onset of Ca alternans preceded the detection of APD alternans. This could be due to subtle APD alternans below our detection threshold (0.6–3 ms), but also could be explained if primary Ca_i transient alternans had balanced effects on Ca-sensitive currents tending to prolong and shorten APD (e.g., Na-Ca exchange and L-type Ca current inactivation, respectively). Although Ca_i-driven alternans might seem less likely in neonatal rat ventricular myocytes because of their immature SR, recent studies have shown that, after several days in culture (equivalent to the time monolayers were studied here), neonatal ventricular myocytes resemble adult ventricular myocytes more closely than freshly dissociated neonatal myocytes, both histologically and functionally with respect to T tubule and SR Ca cycling properties (10, 32).

The mechanism underlying prominent CV restitution observed in the monolayers is unclear. CV restitution is usually attributed to the kinetics of the Na current's recovery from inactivation. In intact 3D ventricular tissue, CV restitution is typically not engaged until very short DIs, consistent with normally rapid Na current recovery kinetics. In monolayers, however, CV varied almost continuously over a wide range of DIs (Fig. 2*D*). Although it is possible that cultured neonatal rat ventricular myocytes have much slower Na channel recovery kinetics than adult ventricular cells, another potential explanation may involve heart rate sensitivity of gap junctional conductance, the other key determinant of CV. During rapid pacing, either intracellular acidosis or elevated Ca_i levels could reduce gap junction conductance and progressively slow CV. The observation that BAY K 8644 exacerbated CV restitution (Fig. 2*D*) is consistent with this possibility, since BAY K increases diastolic Ca_i in chick embryonic myocytes (16), and Cabo et al. (1) reported that BAY K 8644 caused CV slowing due to decreased gap junctional conductance in infarcted hearts. A limitation of our study, however, is that we could not reliably measure changes in diastolic Ca_i in this preparation, as previously noted by Fast et al. (6) in this preparation, although it is possible in other preparations (4, 16).

Spatially Discordant Alternans and Initiation of Reentry

Pastore et al. (18) demonstrated that spatially discordant alternans can produce spatial repolarization gradients steep enough to cause unidirectional conduction block and reentry. We have extended their findings by demonstrating the relevance of the nodal line to the site of conduction block leading to initiation of reentry. Under control conditions, conduction block occurred near the nodal line in 63% of cases. After BAY K 8644, which shortened the spacing between nodal lines, the incidence of conduction block increased and was preceded by spatially discordant alternans in 100% of cases. As predicted theoretically (9, 31) and demonstrated experimentally (Fig. 7*A*), the nodal line marks the location of steepest APD and Ca transient gradients. The APD gradient at the nodal line in Fig. 7*A* reached 6 ms/mm, which agrees well with the experimental estimate of >3.2 ms/mm necessary for conduction block measured in intact ventricular tissue (15), as well as with theoretical predictions (21). In monolayers, nodal lines consistently predicted the location of conduction block, such that block occurred when propagation was in the direction of short-to-long APD (i.e., increasing refractoriness) and small-to-large Ca transient of the previous beat. BAY K 8644 increased the incidence of conduction block by shortening the length scale of spatially discordant alternans, which is equivalent to steepening the spatial APD gradient.

Limitations

At any given pacing rate, APD and Ca_i transient alternans can be either transient or persistent. Any sudden change in heart rate produces transient alternans, which then decays exponentially back to the steady-state APD or Ca_i transient amplitude for the new heart rate, typically with a beat constant of three to four beats (8). For practical reasons, we used a pacing protocol in which pacing cycle length was decreased every eight beats by 20 ms, which may not unequivocally delineate between transient and persistent alternans. Thus it is possible that the alternans induced by our pacing protocol was really transient alternans maintained by the continually increasing pacing rate. To eliminate very transient alternans, we required that alternans, once started, had to persist throughout the remainder of the pacing protocol (or until conduction block occurred), but we cannot state conclusively that the monolayers exhibited truly persistent alternans. However, from the perspective of arrhythmogenesis, the key factor is whether the gradient in refractoriness caused by spatially discordant APD alternans is steep enough, even transiently, to cause conduction block and initiating reentry. Our findings show unequivocally that the gradients in refractoriness achieved during spatially discordant alternans in 2D monolayers, whether transient or persistent, were sufficient to cause conduction block and reentry, especially after BAY K 8644. Nevertheless, neonatal myocytes have different electrophysiology and Ca_i cycling features than adult human ventricular myocytes, so that the relevance to the arrhythmogenic consequences of spatially discordant alternans in humans remains speculative. However, if the fundamental dynamics conferred by APD restitution, Ca_i cycling, and CV restitution play comparable roles in the human heart, they must be considered in the future development of antiarrhythmic therapies.

ACKNOWLEDGMENTS

We thank Yohannes Shiferaw, Zhilin Qu, and Alan Garfinkel for helpful discussions.

GRANTS

This study was supported by the Spanish Society of Cardiology (Electrophysiology Fellowship Grant to C. de Diego), the American Heart Association (Grant 0625048Y to C. de Diego; Grants 0365133Y and 0565149Y to M. Valderrábano), the National Heart, Lung, and Blood Institute (Grants P50 HL52319 and P01 HL078931 to J. N. Weiss), and the Laubisch and Kawata Endowments (to J. N. Weiss).

Present address of M. Valderrábano: Cardiology Division, Methodist DeBakey Heart Center, 6550 Fannin St., Suite 1901, Houston, TX 77030.

REFERENCES

1. **Cabo C, Schmitt H, Wit AL.** New mechanism of antiarrhythmic drug action: increasing L-type calcium current prevents reentrant ventricular tachycardia in the infarcted canine heart. *Circulation* 102: 2417–2425, 2000.
2. **Chudin E, Goldhaber J, Garfinkel A, Weiss J, Kogan B.** Intracellular Ca^{2+} dynamics and the stability of ventricular tachycardia. *Biophys J* 77: 2930–2941, 1999.
3. **Clusin WT.** Mechanisms of calcium transient and action potential alternans in cardiac cells and tissues. *Am J Physiol Heart Circ Physiol* 294: H1–H10, 2008.
4. **Del Nido PJ, Glynn P, Buenaventura P, Salama G, Koretsky AP.** Fluorescence measurement of calcium transients in perfused rabbit heart using rhod 2. *Am J Physiol Heart Circ Physiol* 274: H728–H741, 1998.
5. **Echebarria B, Karma A.** Instability and spatiotemporal dynamics of alternans in paced cardiac tissue. *Phys Rev Lett* 88: 208101, 2002.
6. **Fast VG.** Simultaneous optical imaging of membrane potential and intracellular calcium. *J Electrocardiol* 38: 107–112, 2005.
7. **Fast VG, Cheek ER, Pollard AE, Ideker RE.** Effects of electrical shocks on Ca_i^{2+} and Vm in myocyte cultures. *Circ Res* 94: 1589–1597, 2004.
8. **Franz MR, Swerdlow CD, Liem LB, Schaefer J.** Cycle length dependence of human action potential duration in vivo. *J Clin Invest* 82: 972–979, 1988.
9. **Hayashi H, Shiferaw Y, Sato D, Nihei M, Lin SF, Chen PS, Garfinkel A, Weiss JN, Qu Z.** Dynamic origin of spatially discordant alternans in cardiac tissue. *Biophys J* 92: 448–460, 2007.
10. **Husse B, Wussling M.** Developmental changes of calcium transients and contractility during the cultivation of rat neonatal cardiomyocytes. *Mol Cell Biochem* 163–164: 13–21, 1996.
11. **Karma A.** Electrical alternans and spiral wave breakup in cardiac tissue. *Chaos* 4: 461–472, 1994.
12. **Kuo CS, Munakata K, Reddy CP, Surawicz B.** Characteristics and possible mechanism of ventricular arrhythmia dependent on the dispersion of action potential durations. *Circulation* 67: 1356–1367, 1983.
13. **Laurita KR, Girouard SD, Rosenbaum DS.** Modulation of ventricular repolarization by a premature stimulus: role of epicardial dispersion of repolarization kinetics demonstrated by optical mapping of the intact guinea pig heart. *Circ Res* 79: 493–503, 1996.
14. **Laurita KR, Katra R, Wible B, Wan X, Koo MH.** Transmural heterogeneity of calcium handling in canine. *Circ Res* 92: 668–675, 2003.
15. **Laurita KR, Rosenbaum DS.** Interdependence of modulated dispersion and tissue structure in the mechanism of unidirectional block. *Circ Res* 87: 922–928, 2000.
16. **Lee HC, Clusin WT.** Effect of Bay K8644 on cytosolic calcium transients and contraction in embryonic cardiac ventricular myocytes. *Pflügers Arch* 413: 225–233, 1989.
17. **Nolasco JB, Dahlen RW.** A graphic method for the study of alternation in cardiac action potentials. *J Appl Physiol* 25: 191–196, 1968.
18. **Pastore JM, Girouard SD, Laurita KR, Akar FG, Rosenbaum DS.** Mechanism linking T-wave alternans to the genesis of cardiac fibrillation. *Circulation* 99: 1385–1394, 1999.
19. **Pastore JM, Rosenbaum DS.** Role of structural barriers in the mechanism of alternans-induced reentry. *Circ Res* 87: 1157–1163, 2000.
20. **Pruvot E, Katra RP, Rosenbaum DS, Laurita KR.** Calcium cycling as mechanism of repolarization alternans onset in the intact heart. *Circulation* 106: 191–192, 2002.
21. **Qu Z, Garfinkel A, Weiss JN.** Vulnerable window for conduction block in a one-dimensional cable of cardiac cells. 1. Single extrasystoles. *Biophys J* 91: 793–804, 2006.
22. **Qu Z, Karagueuzian HS, Garfinkel A, Weiss JN.** Effects of Na^+ channel and cell coupling abnormalities on vulnerability to reentry: a

simulation study. *Am J Physiol Heart Circ Physiol* 286: H1310–H1321, 2004.
23. **Qu Z, Garfinkel A, Chen PS, Weiss JN.** Mechanisms of discordant alternans and induction of reentry in simulated cardiac tissue. *Circulation* 102: 1664–1670, 2000.
24. **Rohr S, Scholly DM, Kleber AG.** Patterned growth of neonatal rat heart cells in culture. Morphological and electrophysiological characterization. *Circ Res* 68: 114–130, 1991.
25. **Rosenbaum DS, Jackson LE, Smith JM, Garan H, Ruskin JN, Cohen RJ.** Electrical alternans and vulnerability to ventricular arrhythmias. *N Engl J Med* 330: 235–241, 1994.
26. **Sato D, Shiferaw Y, Garfinkel A, Weiss JN, Qu Z, Karma A.** Spatially discordant alternans in cardiac tissue. Role of calcium cycling. *Circ Res* 99: 520–527, 2006.
27. **Sato D, Shiferaw Y, Qu Z, Garfinkel A, Weiss JN, Karma A.** Inferring the cellular origin of voltage and calcium alternans from the spatial scales of phase reversal during discordant alternans. *Biophys J* 92: L33–L35, 2007.
28. **Shiferaw Y, Karma A.** Turing instability mediated by voltage and calcium diffusion in paced cardiac cells. *Proc Natl Acad Sci USA* 103: 5670–5675, 2006.
29. **Shiferaw Y, Sato D, Karma A.** Coupled dynamics of voltage and calcium in paced cardiac cells. *Phys Rev E Stat Nonlin Soft Matter Phys* 71: 021903, 2005.
30. **Tolkacheva EG, Schaeffer DG, Gauthier DJ, Krassowska W.** Condition for alternans and stability of the 1:1 response pattern in a "memory" model of paced cardiac dynamics. *Phys Rev E Stat Nonlin Soft Matter Phys* 67: 031904, 2003.
31. **Watanabe MA, Fenton FH, Evans SJ, Hastings HM, Karma A.** Mechanisms for discordant alternans. *J Cardiovasc Electrophysiol* 12: 196–206, 2001.
32. **Zimmermann WH, Schneiderbanger K, Schubert P, Didie M, Munzel F, Heubach JF, Kostin S, Neuhuber WL, Eschenhagen T.** Tissue engineering of a differentiated cardiac muscle construct. *Circ Res* 90: 223–230, 2002.